The Physicochemical Mechanisms of the Double Layer Capacitance Dispersion and Dynamics : An Impedance Analysis

Maximilian Schalenbach*, Yasin Emre Durmus, Shay A. Robinson, Hermann Tempel, Hans Kungl, and Rüdiger-A. Eichel

Fundamental Electrochemistry (IEK-9), Institute of Energy and Climate Research, Forschungszentrum Jülich GmbH

52425 Jülich, Germany

*corresponding author: m.schalenbach@fz-juelich.de

KEYWORDS: Impedance spectroscopy, Double Layer Capacitance, Gold.

ABSTRACT: Gold, as the noblest metal, is an appropriate model electrode to study electrochemical double layers. This study examines the frequency dispersion of the double layer of polished gold electrodes in perchloric acid with impedance spectroscopy under amplitude, electrolyte concentration and potential variation. The dynamic perturbation of the double layer equilibrium by impedance measurements shows a constant phase (CP) response (phase angle of approximately -75°) which is responsible for a frequency dispersion of the capacitance. The response is almost independent of the excitation amplitude, for which the CP behavior is ascribed to resistive-capacitive (RC) contributions of the electric field driven ion separation instead of previously reported diffusion limited adsorption processes. The RC character of the double layer in combination with the electrolyte resistance is accompanied by a relaxation that can damp the ion movement and the related ion separation. At the relaxation frequency, the capacitance is found to be independent of the electrolyte concentration, which is attributed to a constant ratio of the contributions of damped ion movement and dielectric polarization of water molecules.

Introduction

Electrochemical reactions take place at interfaces between electrodes and electrolytes, where double layer capacitances (DLCs) affect the spatial distribution of the reaction-driving potential. In electrochemical devices such as batteries[1], electrolyzers[2] or fuel cells[3], DLCs appear as inevitable phenomena that affect the physicochemical reactions in these devices. Direct application of the phenomena of DLCs is found in electrochemical capacitors [4].

Under electrostatic conditions (no current), the electrolyte - like every other conductor - prevents internal electric fields by shielding potential differences at the electrodes in the form of double layers. By applying a varying potential or by inducing a potential driven electrochemical reaction, the electrostatic equilibrium is disturbed and electrochemical currents result. Double layers are described by models[5] that involve contributions from (i) dielectric polarization of the electrolyte solvent, (ii) adsorption of hydrated and non-hydrated ions and (iii) charge separation by the ionic displacement of dissolved ions in the electrolyte close to the electrode.

Basic theories of electrochemical double layers were developed in the beginning of the 20th century[6], with significant contributions by Helmholtz[7], Gouy[8], Chapman[9] and Stern[10]. Later developments include the influence of the electronic structure of the electrode and its potential[11–13], ion adsorption[14,15] and pseudo-capacitive contributions[16,17] with partly outer sphere reaction types[18–20]. The classical models are based on Poisson's law and predict the static ion distribution in the electrolyte under equilibrium conditions. In contrast, the capacitance of the double layer is typically measured under varying electrode potential so that the dynamic changes of the double layer are measured. The thus measured perturbation of equilibrium states are described by different physics as the static properties considered in the theories. As a result, the classic models cannot predict the dynamic properties of the double layer and the related frequency dispersion that is measured by impedance spectroscopy.

Gold, as the noblest of all metals[21], does not form oxides or dissolve in aqueous electrolytes (except aqua regia) within a broad electrochemical and pH window[22,23]. Thus, gold represents a model system to measure DLCs in aqueous solutions and to understand the underlying physical mechanisms. Moreover, the surface polishing of gold is easily accomplished with aqueous polishing agents under atmospheric conditions. Neither hydrogen nor oxygen strongly bond or adsorb on Gold[21], for which its currents in aqueous cyclic voltammetry are far smaller than those of other noble metals such as the platinum metal group[24–26]. Despite these unique characteristics, reported capacitances for gold electrodes in aqueous electrolytes vary from 6 - 100 µF/cm^2 [27–34]. Purely capacitive[27,35]

and constant phase type frequency dispersions[28–31,36,37] with different equivalent circuit diagrams for fitting and physicochemical interpretations are reported.

The aim of this study is to comprehend the broad variation of reported specific double layer capacitances, to understand its frequency dispersion, the physicochemical mechanisms during potentiodynamic probing, and to describe the resistive-capacitive coupling with its relaxation behavior. On the basis of the previously mentioned works, three different equivalent circuits are fit to the measure frequency dispersion of a polycrystalline gold electrode in perchloric acid in order clarify their validly. To further analyze the physicochemical mechanisms of the double layer capacitance, the effect of experimental parameters such as electrolyte concentration, excitation amplitude and electrode potential on the frequency dispersion are examined. With gold as model system, the physical processes that contribute to the double layer of every electrode in aqueous electrolyte are parameterized and their impact on the response is revealed.

Theory

The aim of this section is to describe the calculation of capacitive contributions to the impedance, to present the equivalent circuits that are used to describe the double layer and to discuss the relaxation properties of resistive-capacitive coupling.

Capacitive contributions to the impedance – With reference to classical impedance theory, the impedance of a capacitor C is solely imaginary as described by

$$Z''(\omega) = -\frac{1}{\omega\, C}, \qquad (1)$$

where $\omega = 2\pi f$ denotes the angular frequency of the excitation. In multi component circuits, the imaginary parts of the impedances typically show complicated frequency dependencies. The frequency dependent capacitive contributions $C(\omega)$ to the impedances of such circuits are here defined on the basis of the equation 1 by:

$$C(\omega) = -\frac{1}{\omega\, Z''(\omega)} \qquad (2)$$

Constant phase element (CPE) and charge separation – A CPE describes a frequency independent constant phase angle of the impedance and is typically used to parameterize physicochemical phenomena such as diffusion limitations[38–40] or resistivity distributions in weakly conducting films and porous structures [31,41,42]. The impedance of the CPE[37,41] is described by

$$Z_{\mathrm{CPE}} = \frac{\zeta}{(i\,\omega\,)^n} \qquad (3)$$

where ζ denotes a proportionality factor and n the exponent. With an exponent of $n = 1$, the CPE is purely capacitive while $n = 0$ represent purely resistive contributions. Exponents of $0 < n < 1$ mean a mixture of resistive and capacitive contributions. With an exponent of $n = 0.5$, the CPE equals the Warburg element that is commonly considered as an idealized description of diffusion limitations in electrochemistry[43]. Using the Euler equation in the form of $i^{-n} = \cos(-0.5\,\pi n) + i\sin(-0.5\,\pi n)$, the real and imaginary part of the CPE can be calculated:

$$Z_{\mathrm{CPE}} = \zeta\,\omega^{-n}[\cos(-0.5\,\pi n) + i\sin(-0.5\,\pi n)] \qquad (4)$$

The CPE can be represented by a transition line model in terms of a ladder network of resistances and capacitances[44,45]. A combination of infinitesimal capacitances and resistances is used in this work to describe the spatial charge separation of ions that are moved by the applied potential perturbation during impedance measurements. For this interpretation, the resistive contributions are associated with the ion movement from the decaying electric field in the double layer while the capacitive contributions are displayed by the reversible charge separation in the double layer and the polarization of water molecules.

Because the charge separation and the diffusion limited adsorption are both described by CPEs, one might falsely assign a CPE behavior to either one or the other contribution. As capacitances and Ohmic drops are themselves characterized by a linear response to the excitation amplitude, the response of the charge separation is expected to be linear as well. In contrast, diffusion limitations typically are characterized by a non-linear response as the diffusion limitations increase towards higher excitation amplitudes. Hence, the effect of excitation amplitude on both mechanisms is profoundly different while their frequency dependence can be similar.

Equivalent circuits – The most frequently used circuit in electrochemistry is the Randles circuit[46], where the double layer is parameterized by a capacitance for dielectric contributions, which is parallel to a charge transfer resistance in serial combination with a constant phase element (CPE) that describes diffusion limited adsorption or Redox processes. In this work, diffusion limited charge transfer processes are neglected for the considered gold electrode as these are later shown to negligibly contribute to the overall response. Circuit (i) in Fig 1 consists of a series combination of the electrolyte resistance R_{S} with a capacitance C_S that represents the double layer (to be understood as a superposition of different physicochemical mechanisms). The impedance of the real and imaginary part of circuit (i) can be described by $Z' = R_{\mathrm{S}}$ and equation 1 for the relation of capacitance and imaginary part of the impedance.

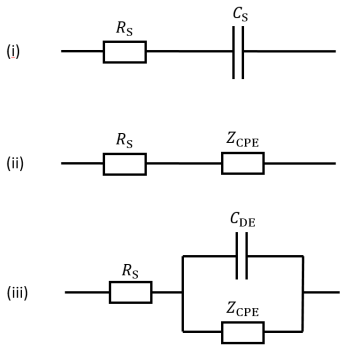

Fig. 1: Equivalent circuits used to parameterize the electrode. (i): Series connection of the electrolyte resistance R_s and a capacitance C_S that serves as a simple parameterization of the double layer. (ii) The charge separation by ion displacement in the double layer is represented by a constant phase element Z_{CPE} that describes mixed resistive-capacitive contributions. (iii) The capacitance C_{DE} describes the dielectric contributions by the polarization of water molecules to the response.

In circuit (ii), a CPE describes the coupling of resistive and capacitive contributions that are caused by the potential driven charge separation in the double layer. The overall impedance of circuit (ii) can be calculated by including the electrolyte resistance:

$$Z = R_{\mathrm{S}} + Z_{\mathrm{CPE}} \tag{5}$$

The capacitive contributions of this circuit to the impedance are described by:

$$C(\omega) = -\frac{1}{\zeta\ \omega^{-n+1} \sin(-0.5\ \pi n)} \tag{6}$$

In circuit (iii), the dielectric contributions by the polarization of water molecules are included. A frequency independent constant polarization loss was previously reported for the dielectric properties of solids[47] and related to the CPE behavior of the double layer of aqueous solutions[40]. However, the dielectric loss of water at the considered frequencies is negligible as relaxation frequencies of water molecules are in the range of microwaves[48] for which these processes are believed to contribute in a purely capacitive nature. Accordingly, the dielectric processes are parameterized by the capacitance C_{DE} for which the impedance of circuit (iii) can be described by:

$$Z = R_{\mathrm{S}} + \frac{1}{(Z_{\mathrm{CPE}})^{-1} + i\omega C_{\mathrm{DE}}} \tag{7}$$

On the basis of the calculated imaginary part, the capacitive contributions can be derived (with $\alpha = -n$) as:

$$\mathrm{C}(\omega) = C_{\mathrm{DE}} + \frac{\frac{1}{\omega} - C_{\mathrm{DE}}\,\xi \sin\left(\frac{\pi\alpha}{2}\right)\omega^{\alpha}}{-\xi \sin\left(\frac{\pi\alpha}{2}\right)\omega^{\alpha} + \left[\left(\xi \cos\left(\frac{\pi\alpha}{2}\right)\omega^{\alpha}\right)^{2} + \left(\xi \sin\left(\frac{\pi\alpha}{2}\right)\omega^{\alpha}\right)^{2}\right]} \tag{8}$$

Similar to the dielectric contributions, capacitive ion movement is also characterized by high frequency relaxation properties[49]. Thus, the mechanisms themselves are expected to be independent of the frequency within the window of 0.01 Hz to 100 kHz that is typically applied in electrochemical impedance spectroscopy.

Relaxation - A relaxation describes the change from a perturbed state to equilibrium with a damping that leads to a characteristic time delay. In the case of RC circuits such as circuit (i), an applied voltage can act as an external force that perturbates equilibrium by charging/discharging the capacitor, while the resistor damps the current by means of an Ohmic drop. The characteristic time delay can be related to the frequency domain as described by the relaxation frequency f_r:

$$f_r = \frac{1}{2\pi\ R_S\ C_S} \tag{9}$$

At frequencies that are far smaller than the relaxation frequency of the RC series circuit, the impedance is high and the currents are small, so that the damping by the Ohmic drop plays a minor role. The system follows more or less instantaneously the excitation, which means quasi-equilibrium states during the perturbation. Towards higher frequencies the impedance of the capacitance decreases, so that the currents caused by the potential excitation increase. These higher currents increase the resistive contributions to the overall response. At the relaxation frequency, the resistive and capacitive contributions affect the impedance equally and the phase angle is 45°. In this case, the system is characterized by a delayed and damped response. The relaxation properties of circuit (i) will later serve as an approximation of those of the other circuits.

Methods

A custom polypropylene cell was used for the electrochemical measurements, where a geometrical surface area 0.78 cm² (circular shape with 1 cm diameter) of the working electrode was exposed to the electrolyte. As illustrated in Fig 2, the working electrode in the form of a cold rolled gold plate (Junker Edelmetalle GmbH, purity 99.99%) is aligned parallel to a gold wire coil that served as the counter electrode. A Luggin-capillary was placed with a distance of approximately 4 mm to the working electrode. The capillary is connected to a separated compartment with an Ag/AgCl reference electrode (Metrohm, 3 M KCl). A separated glass inset with a frit was used to prevent hydrogen or oxygen evolved by electrolyte decomposition at the counter electrode from diffusing to the working electrode. The cell was sealed with a silicone ring that held the glass inset, and the interior was purged with argon at a rate of 50 ml/min for a minimum of one hour prior to the impedance measurements in order to reduce the concentration of dissolved oxygen in the electrolyte. The impedance spectra were recorded using either a Biologic VMP-3 (16 channel screening device) or an Autolab Modular Line potentiostat (high precision single channel device). These different potentiostats were intentionally used to elucidate measurement errors in detail.

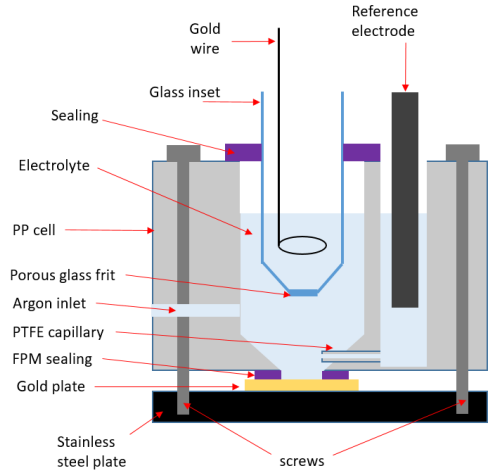

Fig. 2: Schematic sketch of the electrochemical cell used for all impedance measurements. PP: Polypropylene. PTFE: Polytetrafluoroethylene. FPM: Fluoroelastomer.

Before measuring, the surface of the gold plate was cleaned by polishing with 4000 grid SiC paper (Struers). Subsequently, it was additionally polished for 5 min with different soft polishing cloth (Struers) that were individually loaded with diamond particles of 1, 0.25 and 0.05 µm diameter (Struers) and water as lubricant, so that a mirror finish was obtained. This was done using a Struers Tegramin polishing machine with an applied pressure of 10 N and a rotation speed of 200 rpm. After polishing, the surface was thoroughly cleaned with acetone and afterwards rinsed with water to remove any residual polishing solution. Finally, the surface was polished with soft absorbent cotton and rinsed with water again. A poorly polished surface will increase the measured capacitances, so it is highly important that this procedure is conducted thoroughly in order to obtain reproducible electrochemical data.

The electrolytes for the electrochemical measurements were composed of deionized water (resistance of 18.2 MΩcm, Veolia Pureflex) with perchloric acid (Suprapur, Merck chemicals). The potentials stated in this article are referring to the reversible hydrogen electrode reference, which was calculated by the measured potential plus the potential of the Ag/AgCl electrode of 0.197 V *vs.* SHE and 59 mV per tenfold of proton concentration. Before an impedance spectrum was measured, cyclic voltammetry from 0 to 1 V *vs.* RHE was conducted to oxidize/reduce adsorbents from previous air exposure and to ensure reproducible starting conditions of the electrode. The mean potential of the excitation was applied for 120 s to reduce charge or de-charge currents. Unless stated otherwise, peak-to-peak excitation amplitudes of 10 mV were employed.

Results and Discussion

All impedance data shown in this work were obtained on a polished gold electrode in an Argon purged electrolyte. A constant potential was applied for at least for 120 s to decrease charging or decharging currents to negligible contributions in the nano-Amps regime (same scale as the noise). After such a quasi-equilibrium was reached, the potential perturbations by the impedance measurement were applied. Accordingly, the dynamics of nearly equilibrated states in the double layer were measured.

Evaluation of the impedance spectra

Fig 3 shows the impedance data of a polished gold sample in 0.1 M $HClO_4$, including the real and imaginary parts of the impedance, the phase angle θ and the capacitive contributions $C(f)$ as determined by equation 2. In order to show the effect of measurement errors, the data of two different potentiostats (a Biologic VMP-3 and an Autolab Modular Line) were compared. The frequency range in which the data of both impedance analyzers agrees ensures the reliability of the experimental data, while the frequencies with deviations in the data show the error in measurement. The figure also shows the fits of circuits (i), (ii) and (iii) to the data of the Autolab potentiostat. The differences between the fits are observed in the real and imaginary parts of the impedance and can be seen more clearly in the phase angle and capacitive contributions; therefore, this will be the focus of the following evaluation.

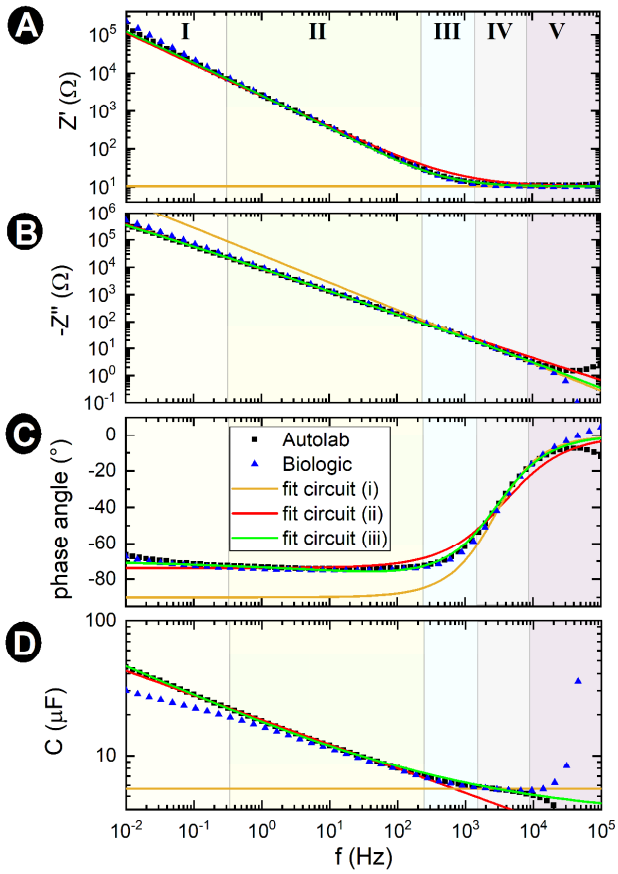

Fig. 3: Impedance measurement (scatter) of the polished gold sample at 0.5 V vs RHE, 0.01 V amplitude and 0.1 M $HClO_4$ electrolyte. Fit of circuit (i) (brownish solid line), of circuit (ii) (red solid line) and circuit (iii) (green solid line). (A): Real part of the impedance. (B) Negative imaginary part. (C): Phase angle in degrees. (D) Capacitive contributions to the impedance. The regions I, II, III, IV and V with colored shadings are used to discuss the frequency dependence (see text).

The impedance spectra covers seven decades of frequency, thus it is useful to separate the spectra into different regions with different physical meanings. Here, five regions (shaded with different colors in Fig 3), that are distinguished by the information contained in the phase angle, are used. Before elucidating the properties of each region in detail, two groups can be formed: At the very low frequencies (region I) and very high frequencies (region V) of the spectrum, measurement errors lead to deviations of the capacitive contribution to the impedance recorded with the two different impedance analyzers. In between these regions, reliable information on the double layer can be obtained.

To fit the parameters of the different circuits to the impedance data, the following procedure was used: The electrolyte resistance (R_s) was obtained from the high frequency component of the real part of the impedance in region (V) without a fit as $R_S = 10.5\ \Omega$. In the case of circuit (i), the only remaining fit parameter is the capacitance C_S, which was determined from the measured $C(\omega)$ at the relaxation frequency of the RC circuit (where the phase angle equals -45°). This capacitance of $C_S = 5.8\ \mu F$ at $f_r = 2.24$ kHz is a superposition of different mechanisms and does not represent a single direct physical component, however, it will be used to characterize the relaxation properties of the response in this frequency regime. The two open parameters of circuit (ii) are fit to the data in region (II), yielding $n = 0.77$ and $\xi = 47634$. As only two parameters must be fit to the data (R_S extracted from the high frequency resistance), this fit is reproducible and unambiguous. However, fitting with two open parameters can run into local minima, for which the exponent n was varied in 0.005 steps from 0.7 to 0.85 while the parameter ξ was fit in Python (see supporting information for the computer code). The mean quadratic deviation to the measurement was calculated for each fit of the different n values, and the parameters with the lowest quadratic deviation were chosen as the best ones. The fit of circuit (iii) was conducted with a capacitance of $C_{\mathrm{DE}} = 3.5\ \mu F$ and again ξ and n as open parameters. This value of C_{DE} was found by iterative probing, leading to the best agreement between the fit and the measured data. The fitting procedure is reproducible and unambiguous, as each parameter has a decisive impact on the capacitance and phase angle dispersion.

The residuals of the different fits are graphed in Fig. 4. Circuit (iii) matches from regions (I) to (IV) within a 5 % deviation from the experimental data, while the other circuits agree only in small frequency ranges. As circuit (iii) comes with only one more parameter as circuit (ii), it holds the minimum amount of parameters required to represent the data of the full frequency range and the maximum amount of parameters to obtain unambiguous results.

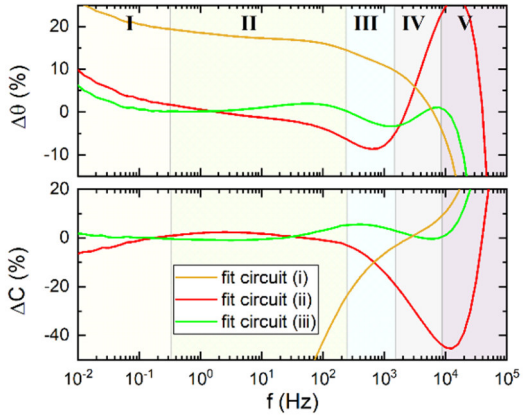

Fig. 4: Fit residuals as percentage differences. Top: Phase angle. Bottom: Capacitance. Circuit (i) just agrees with the experimental data in region (IV), while circuit (ii) agrees with the data in region (I) and (II). Circuit (iii) agrees with the full spectra excluding region (V) that is dominated by measurement error.

In the following, the fits and the physical processes in the five different regions will be described in more detail:

Region (V) – This region describes the high frequency probing, where the phase angle approaches zero as the electrolyte resistance dominates the response. The capacitive contributions to the impedance are affected by large measurement errors, which is reflected by the diverging capacitive contributions as measured by the two different impedance analyzers employed. The value of the impedance Z and the phase angle θ are measured by lock-in-amplification in impedance analyzers, from which the imaginary part is calculated by $Z'' = Z \sin(\theta)$. At small values of θ, the approximation $\sin(\theta) \approx \theta$ is valid, which means that the measurement error of θ directly affects the error of the imaginary part of the impedance. For example, if $\theta = 2° \pm 1°$, the relative error of Z'' is $\pm 50\ \%$, while in the case of $\theta = 45° \pm 1°$ the error of Z'' is just $\pm 2\ \%$,. Accordingly, the relative measurement error of Z'' increases towards low absolute values of the phase angle. Moreover, inductive contributions affect Z'' linearly with frequency and thus complicate the estimated capacitance at high frequencies. With reference to equation 2, the error of Z'' directly influences the error of the capacitive contributions to the impedance, and thus are not reliable in this region.

Region (IV) – Here the phase angle ranges from -20 to $-60°$, for which its absolute values are small enough to enable a precise determination of the imaginary part of the impedance. The lowest reliable value of the capacitive contributions can be measured in this region as they increase towards lower frequencies. Moreover, this region contains the resistive-capacitive relaxation with a relaxation frequency f_r at $-45°$. The fit of circuit (i) reasonably describes the data with maximum residuals of $\pm 12\%$. Thus, circuit (i) can serve in this frequency range as an approximation of the experimental data and the resistive-capacitive relaxation properties of the response. The values of the fit of circuit (ii) are too small, while the additional capacitance of circuit (iii) compensates for this.

Region (III) – The phase angle decreases towards lower frequencies as the share of the electrolyte resistance to the overall response is reduced due to smaller currents. Circuit (i) no longer represents the data. The capacitive dominance changes the phase angle towards −90° while the experimental data shows higher phase angles. The agreement with circuit (ii) increases towards lower frequencies.

Region (II) – The CPE dominates the response, for which the phase angle is with approximately −76° almost independent of the frequency as described by circuit (ii). In this frequency region the currents are small, resulting in a negligible impact of the Ohmic drop at the electrolyte resistance on the overall response. The capacitance of circuit (iii) has a small impact on the response in this regime, for which the frequency dependence of circuit (ii) and circuit (iii) are similar.

Region (I) – In this low frequency region, the impedance approaches the MΩ range, for which currents become small and measurement errors increase. As a result, the data of both impedance analyzers show significant differences. Moreover, higher harmonics and related non-linear contributions to the impedance (that are typically capacitive and smoothed at higher frequencies) increase the measurement error at these low frequencies. In addition, as the currents become small, the relative contribution of parasitic reactions, such as the reduction of oxygen impurities, increase. Such parasitic reactions are mainly Ohmic and hence increase the phase angle.

To summarize, the parametrization of the double layer by a capacitance in combination with a CPE led to a good agreement with the reliable (excluding region V) measured data, and the resistive-capacitive coupling in this circuit leads to a relaxation.

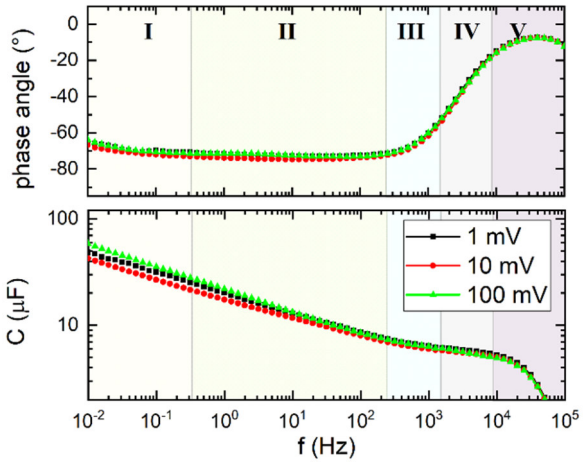

Fig. 5: Impedance spectra under amplitude variation in 0.1 M at 0.5 V *vs* RHE. The differences of the responses are within the measurement precision negligible, which means an approximately linear response. A constant phase behavior with a linear response is displayed by the resistive-capacitive ion separation.

Amplitude variation

Fig. 5 shows the phase angle and capacitance obtained from individual impedance spectra that were recorded with amplitudes of 1, 10 and 100 mV of the polished gold sample in 0.1 M $HClO_4$ using the Autolab potentiostat. The data with the different amplitudes shows a maximum difference of 20% and not a clear trend as the values of 1 mV measurement is between those of the higher amplitudes. Accordingly, the capacitance can be approximated as independent of the excitation amplitude, which means that amount of charge exchanged and the associated current are approximately linear with the excitation amplitude.

If diffusion limited adsorption is responsible for the CPE behavior, the current would not or minimally change with amplitude. Thus, diffusion limitations would result in a non-linear response with an increasing impedance towards higher amplitudes. In contrast, the resistive-capacitive spatial ion separation and the dielectric contributions are both expected to come with a linear response to the excitation amplitude. The resistive-capacitive ion movement can be described by the transition line model of an infinitesimal ladder network of resistances and capacitances , which was related to the CP behavior in previous works [44,45].

Based on the measured linear response at different amplitudes, capacitive ion separation and the dielectric contributions are shown to dominate the response. In this respect, the potential perturbation is the driving force for the ion movement and their displacement at the electrode. Diffusion partly compensates the movement of separated ions at the interface as it directs them in the opposing direction to the charge separation introduced by the electric field. In this manner, diffusion and ion separation form a temporary equilibrium that shields the electrode potential during the perturbation imposed by the impedance measurement.

Description of the physicochemical processes

Based on the data in Fig. 5, the dielectric polarization and the resistive-capacitive ion movement were discussed to dominate the response. These physicochemical processes are schematically sketched in Fig. 6 for three cases: (A) An equilibrium at a potential of 0.5 V, which was used for most of the measurements in this work. This potential is approximately 0.3 V above the open circuit potential (OCP) that was measured to 0.2 V. The OCP can vary from sample to sample as it can be influenced by impurities or the electrode history. (B) A perturbation by an increase of 0.1 V and (C) a perturbation by a potential decrease of -0.1 V.

At the OPC, the charges in the double layer are assumed to be balanced as no external potential is applied that could drive the charge carrier separation. Equal amounts of positively and negatively charged ions in the double layer are the result of the equilibration. As the applied potential in case A is above the OCP, it separates the charged ions in the double layer. More negative than positively charged ions are close to the working electrode in the double layer in order to balance the potential gradient between the electrode and the electrolyte. The potential gradient orientates the water molecules in the double layer, which results in a mean polarization $\vec{P}$. The water molecules that are attached to the solvation shells of the ions might come with different polarization dynamics as the ones which are surrounded by other water molecules. The constant potential leads to an equilibrium, in which no net ion movement appears and the theories on the electrostatically

shielding (see introduction) can be applied to describe the ion arrangement in the double layer.

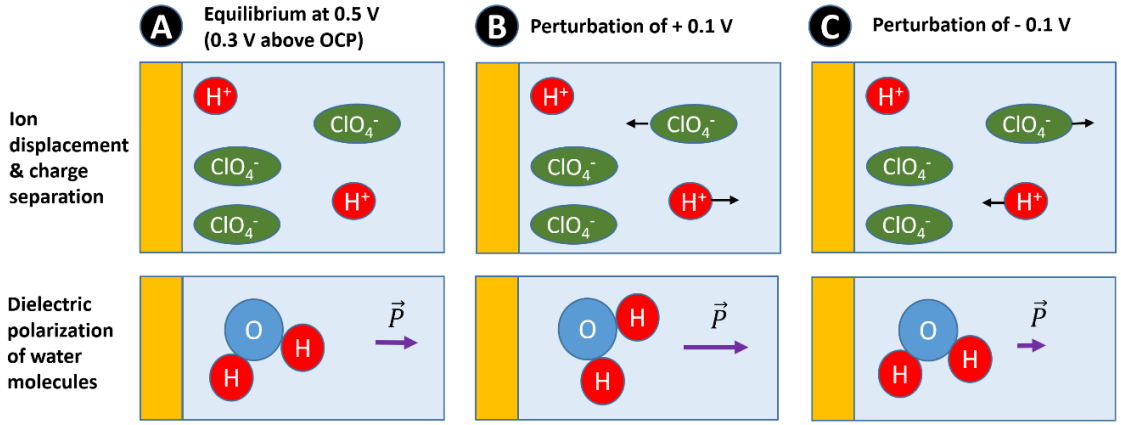

Fig. 6: Schematic sketch of the physicochemical mechanisms of the charge separation (top row) and the dielectric polarization of water molecules (bottom row) for three cases (A, B and C) of applied potentials. The gold electrode is illustrated yellowish, the electrolyte bluish. The open circuit potential (OCP) was measured to approx. 0.2 V, while the equilibrium potential of the illustrated cases is 0.5 V. The black arrows in the top row indicate potential driven ion movement whereas the purple arrows in the bottom row indicate the mean polarization $\vec{P}$ of the water molecules.

When the applied potential is increased as sketched in case (B), the equilibrium is disturbed and the ionic charges start to move. The ratio of negatively charged to positively ions directly at the electrode increases in order to shield the more positive electrode potential. Moreover, due to the increased potential gradient that penetrates into the electrolyte the mean polarization of the water increases as more water molecules are orientated. When the potential is decreased as illustrated in case (C), the ions move in the other directions. The electrode potential comes closer to the OCP, so that the charge ratio of ions close to the electrode becomes more evened out. As the potential gradient in the electrolyte decreases, the mean polarization of the water molecules also decreases.

Electrolyte concentration and relaxation properties

Fig. 7 shows the impedance spectra measured with the Autolab potentiostat (10 mV excitation amplitude) and four different electrolyte concentrations: 0.001, 0.01, 0.1 and 1 M perchloric acid. Each spectra shows similar behavior to the previous presented spectrum with the as discussed five different regions, respectively. The characteristic frequencies of the five different regions shift with approximate proportionality to the electrolyte concentration. To understand this behavior in more detail, the relaxation properties in region (IV) will be a central part of the following discussion. The relaxation frequencies that refer to a phase angle of -45° are marked with vertical dotted lines in Fig. 7. Following the above described procedure, fits of circuit (iii) were conducted to each of the spectra. The open circuit potentials of the gold sample were 0.45, 0.34, 0.22 and 0.06 V *vs.* RHE (error of approximately 0.05 V) for the 0.001, 0.01, 0.1 and 1 M perchloric acid solutions, respectively.

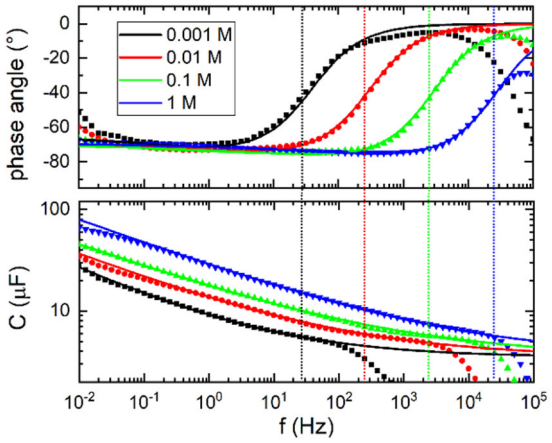

Fig. 7: Impedance on the polished gold plate under varying concentration of perchloric acid at 0.5V vs RHE. Scatter: Experimental data. Solid lines: Fit of circuit (iii). The vertical dotted lines mark the relaxation frequencies at a phase angle of -45°, which are approximately inversely proportional to the electrolyte resistance according to equation 9.

Table 1: *Fit parameters and relaxation properties. The experimentally determined relaxation properties were read out at a phase angle of -45° in region (III) of the impedance spectra and are marked with a "-45°" subscript. The relaxation frequency f_r is calculated from equation 9 from the measured electrolyte resistance and $C_{-45°}$, while Δf denotes the percentage difference of f_r and $f_{-45°}$.*

c (M)	R_S (Ω)	C_{DE} (µF)	ξ (Ω)	n	$f_{-45°}$ (Hz)	$C_{-45°}$ (µF)	f_r (Hz)	Δf (%)
1	1.35	3.5	26865	0.765	2.14E+04	5.79	2.04E+04	-5.0
0.1	10.5	3.5	47634	0.770	2.24E+03	5.80	2.49E+03	10.0
0.01	101	3.5	64126	0.750	2.19E+02	6.04	2.61E+02	16.3
0.001	870	3.5	104885	0.705	2.74E+01	5.54	3.30E+01	16.9

Fehler! Textmarke nicht definiert. Table 1 shows the fit parameters of circuit (III) to each spectrum. As expected, the electrolyte resistance decreases approximately with inverse proportionality to the electrolyte concentration, and a slight increase of the resistance at 1 M is also expected from the ion-ion interaction that leads to deviations from the idealized behavior of infinite solutions [2]. The electrolyte resistance changes also approximately linearly with the electrolyte concentration from 1.35 Ω at 1 M to 870 Ω at 0.001 M. The permittivity of aqueous electrolytic solution only slightly depends on the electrolyte concentration [50,51], so that the dielectric capacitance C_{DE} is assumed to be equal for all the different electrolyte concentrations used here. The differences of the CPE parameters ξ and n for the individual electrolyte concentrations are indicative of the changing interaction of the resistive-capacitive ion separation.

The relaxation frequency as previously described by equation 9 shows that the relaxation frequency is expected to increase proportionally with the electrolyte concentration. The frequencies of the individual spectra at which the phase angle in region (IV) equals -45° are denoted as $f_{-45°}$ and serve as estimations of the relaxation frequencies. This frequency undergoes an approximately proportional linear shift with electrolyte concentration, from 27 Hz at 0.001 M to 21 kHz at 1 M. The capacitance at $f_{-45°}$ is denoted by $C_{-45°}$ and remains nearly constant with values from 5.5 µF at 0.001 M to 5.8 µF at 1 M. In region (IV), circuit (i) was found to be a good approximation for the response, for which its relaxation properties can be used as an approximation for those of circuit (iii). Using equation 9, the relaxation frequency f_r can be calculated from the capacitance and the electrolyte resistance. Hereto, $C_{-45°}$ serves as an estimation for the capacitive contributions. By comparing the calculated relaxation frequency f_r and the estimated relaxation frequency $f_{-45°}$, the quality of the approximation can be controlled. The percentage difference between both frequencies is denoted as Δf and also summarized in Table 1. The values of Δf range between -5% and 17%. Accordingly, an estimation of f_r by $f_{-45°}$ is reasonable.

As with the frequency of the relaxation, the frequencies that describe the other four regions (Fig. 3) of the spectra change to the same extent with the electrolyte concentration. Accordingly, as expected the onset frequencies of region V with the diverging capacitances change proportionally to the electrolyte concentration. An exception of the linear frequency change of the regions is given by region I, where the low frequencies lead to non-linear responses and small currents. Hence, in this region the data becomes independent of the concentration less reliable and deviations from the fit arise. The above mentioned reduction of oxygen impurities might also lead to an increasing phase angle for the smallest currents measured (at low frequencies and low ionic concentrations).

At frequencies close to the relaxation frequency, the electric-field driven ion movement is strongly damped as the time delay to the response is in the same time scale as that of the perturbation period. Towards higher frequencies the damping increases and the ion movement caused by the perturbation becomes negligible. As a result, the contributions of the spatial ion separation to the capacitive response is weakened and the impact of the dielectric contributions becomes significant. Table 1 shows that at the relaxation frequency the capacitive contributions to the impedance are almost independent of the electrolyte concentration. This almost constant value of the capacitance is attributable to a constant ratio of the capacitive contributions of strongly damped charge separation (parameterized by the CPE) and the dielectric background of the polarizable water molecules (parameterized by C_{DE}). Accordingly, the electrode capacitance can be reproducibly measured at the RC-relaxation frequency independent of the electrolyte concentration.

Bockris *et al.* [52] discussed that the frequency dispersion of DLCs is attributable to the dielectric properties of the water molecules and their relaxation. However, the dielectric relaxation of water molecules takes place in the microwave frequency range[48]. Moreover, this interpretation by [52] cannot explain the concentration dependence of the capacitance dispersion, for which an interpretation of the ionic movement and its related resistive contributions seems more likely. Useful information on the double layer can be obtained from at and below the relaxation frequency, for which experimentalists should thoroughly choose the frequency range to obtain data on the double layer.

Effect of electrode potential

Thus far, the frequency dependence of the capacitive contributions to the impedance was considered, where the absolute values of the capacitance matter for the properties of the relaxation. The following evaluation focuses on the impact of electrode potential on the capacitive contributions, where the relaxation properties play a minor role. Specific capacitances (normalized to surface area) are commonly used to compare different samples and will also be used in the following. The geometric surface area of the polished sample is approximated as the electrochemically active surface area of the sample that is exposed to the electrolyte.

Fig. 8 shows the potential dependence of the specific capacitive contributions to the impedance of the polished gold plate at a concentration of 0.1 M $HClO_4$. Individual impedance spectra were recorded at potentials from 0 to 1.2 V with a 0.1 V increment. The impedance spectra at the different potentials resembled the ones presented, whereas the deviations from the CP behavior in region I slightly varied. The surface area normalized capacitive contributions to the impedance are shown for one frequency per decade from 1 Hz to 10 kHz. In addition, the capacitance at the relaxation frequency of 2.2 kHz is included. In the SI, cyclic voltammetry data on the electrode is also graphed. However, while the impedance probes the perturbation of a nearly equilibrated double layer with small amplitudes, cyclic voltammetry with large amplitudes lead to drastic potential induced changes in the double layer. Thus, the potential dependent data of both techniques cannot be directly compared.

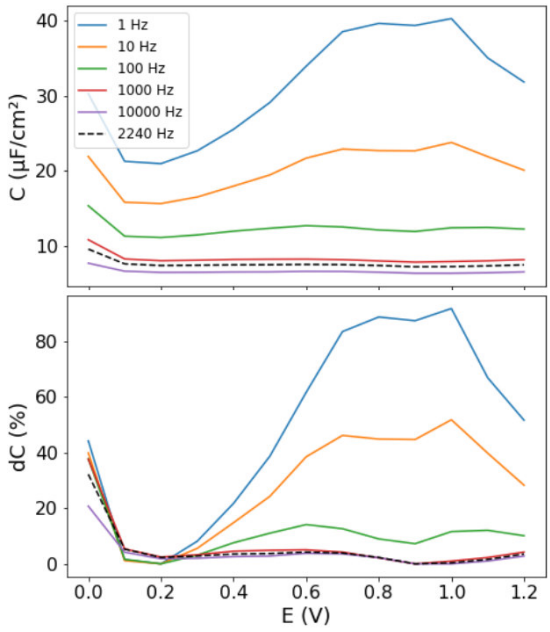

Fig. 8: Top: Specific capacitance as a function of potential for six characteristic frequencies. Data extracted from individual impedance spectra of electrode potentials from 0 to 1.2 V. The frequency of 2240 Hz represents the relaxation frequency. Bottom: Percentage of the potential impact on the capacitance. Hereto, the lowest measured capacitance at the considered frequency was used to normalize the data from the top graph.

The impedance spectra above shows that the capacitance increases towards lower frequencies as the contributions of the spatial ion separation becomes larger. This increase is between 0.3 V and 1.2 V and is significantly larger than at 0.2 V. The value of the electrode potential changes the electrostatic shielding in the double layer and the related spatial ion arrangement near the electrode. In terms of Fig. 6, the ion arrangement at the equilibrium changes with the potential as the ionic charges are moved when the potential is altered. This arrangement of the ions influences the dynamics of the ion separation that is probed by the potential perturbation during impedance measurements and the resulting capacitive response.

At the relaxation frequency (2.2 kHz), the specific capacitance is approximately constant with a value of 7.5 $\pm$ 0.3 µF/cm^2 for potentials between 0.1 and 1.2 V. At 0 V, the capacitance is significantly higher, which might originate from potential driven hydrogen adsorption and desorption. The dielectric contributions from the orientation of water molecules is expected to be independent from potential. As discussed above in detail, the ratio of the capacitive contributions of spatial ion separation and dielectric permittivity to the response are reproducible at the relaxation frequency, as the damping reduces the impact of spatial ion separation on the response. Thus, a change of the ion arrangement by different electrode potentials is expected and is observed to negligibly change the capacitance at the relaxation frequency.

Conclusion

In this study, the physical mechanisms in the double layer are analyzed by impedance spectroscopy on polished gold electrodes. Fits of different equivalent circuits that describe the resistive-capacitive charge separation by ion displacement (parameterized by a constant phase element) and the dielectric permittivity (parameterized by a capacitance) are provided. A combination of both effects is sufficient to describe the impedance spectra over the frequency range that yields reliable data. With the systematic parameter screening of frequency and electrolyte concentration, the entire range of previously reported specific capacitances of gold electrodes from 6 to 100 µF/cm^2 is reproduced. The impedance of the gold electrode is almost independent of the excitation amplitude for which the non-linear response of diffusion limited adsorption processes is found to negligibly contribute to the measured spectra. Instead, the observed constant phase behavior is attributed to the resistive-capacitive coupling of the potential driven dynamic change of the spatial ion arrangement/separation. By damping the ion movement, resistive contributions result in an intrinsic frequency dispersion of the DLC that changes with electrolyte conductivity. At the relaxation frequency of the RC-coupling, ion movement is slowed, so that dielectric contributions to the capacitive response become the dominating mechanism. The capacitance at the relaxation frequency is independent of the electrolyte concentration from 0.001 M to 1 M and the potential from 0.1 to 1.2 V, which is attributed to a constant ratio of the dielectric contributions and ion displacement to the capacitive response. As predicted by theory, the relaxation frequency changes approximately linearly with the electrolyte concentration. At lower frequen-

cies, the capacitive contributions depend on the electrode potential. This influences the static ion arrangement near the electrode and it is this dynamic change that is probed by impedance.

The polished gold electrodes examined in this study serve as a model system to describe the basic physicochemical effects in the double layer that contribute to every electrode, whereas additional phenomena such as specific adsorption are expected for other electrolytes and electrodes. A broad screening of the capacitance dispersion of different materials and electrolytes might be helpful to better understand all physicochemical effects in the double layer. The spatial ion displacement in the double layer affects every electrochemical reaction, however, its detailed impact still has to be resolved. To understand the dynamics in the double layer and the related impedance spectra in more detail, it would be desirable to measure the potential driven ion separation with a spatially resolved technique, however, the small penetration depth is experimentally challenging. Overall, the DLC cannot be considered as a constant, it is a variable with a multidimensional parameter dependency, and this work has moved to clarify this point.

Supporting information

The supporting information to this work contains the derivation of the analytical expression for the impedance of circuit (iii), a cyclic voltammogram of the polished gold sample and computer codes (Python) to fit the circuits to the capacitance dispersion.

Acknowledgement

This work was supported by the German Federal Ministry of Education and Research (BMBF) within the Project iNew (03SF0589A).

References

(1) Armand, M.; Tarascon, J. M. Building Better Batteries. *Nature* **2008**, *451* (7179), 652–657

(2) Schalenbach, M.; Zeradjanin, A. R.; Kasian, O.; Cherevko, S.; Mayrhofer, K. J. J. A Perspective on Low-Temperature Water Electrolysis – Challenges in Alkaline and Acidic Technology. *Int. J. Electrochem. Sci.* **2018**, *13*, 1173–1226

(3) Haile, S. M. Fuel Cell Materials and Components. *Acta Mater.* **2003**, *51* (19), 5981–6000

(4) Wang, Y.; Song, Y.; Xia, Y. Electrochemical Capacitors: Mechanism, Materials, Systems, Characterization and Applications. *Chem. Soc. Rev.* **2016**, *45* (21), 5925–5950

(5) Schmickler, W.; Henderson, D. New Models for the Structure of the Electrochemical Interface. *Prog. Surf. Sci.* **1986**, *22* (4), 323–419

(6) Damaskin, B. B.; Petrii, O. A. Historical Development of Theories of the Electrochemical Double Layer. *J. Solid State Electrochem.* **2011**, *15* (7–8), 1317–1334

(7) Helmholtz, H. Studien Über Electrische Grenzschichten. *Ann. der Phys. und Chemie* **1879**, *7*, 22.

(8) Gouy, M. Sur La Constitution de La Charge Électrique à La Surface d'un Électrolyte. *J. Phys. Théorique Appliquée* **1910**, *9* (1), 457–468

(9) Chapman, D. L. A Contribution to the Theory of Electrocapillarity. *London, Edinburgh, Dublin Philos. Mag. J. Sci.* **1913**, *25* (148), 475–481

(10) Stern, O. Zur Theorie Der Elektrolytischen Doppelschicht. *Zeitschrift für Elektrochemie und Angew. Phys. Chemie* **1924**, *30* (21-22), 508–516

(11) Schmickler, W. Electronic Effects in the Electric Double Layer. *Chem. Rev.* **1996**, *96* (8), 3177–3200

(12) Schmickler, W. A JELLIUM-DIPOLE MODEL FOR THE DOUBLE LAYER. *J. ElectroanaL Chem.* **1983**, *150*, 19–24.

(13) Groß, A.; Sakong, S. Modelling the Electric Double Layer at Electrode/Electrolyte Interfaces. *Curr. Opin. Electrochem.* **2019**, *14*, 1–6.

(14) Biesheuvel, P. M.; Van Limpt, B.; Van Der Wal, A. Dynamic Adsorption/Desorption Process Model for Capacitive Deionization. *J. Phys. Chem. C* **2009**, *113* (14), 5636–5640

(15) Trefalt, G.; Behrens, S. H.; Borkovec, M. Charge Regulation in the Electrical Double Layer: Ion Adsorption and Surface Interactions. *Langmuir* **2016**, *32* (2), 380–400

(16) Brousse, T.; Bélanger, D.; Long, J. W. To Be or Not to Be Pseudocapacitive? *J. Electrochem. Soc.* **2015**, *162* (5), A5185–A5189

(17) Conway, B. E.; Gileadi, E. Kinetic Theory of Pseudo-Capacitance and Electrode Reactions at Appreciable Surface Coverage. *Trans. Faraday Soc.* **1962**, *58*, 2493–2509

(18) Marcus, R. A. On the Theory of Oxidation-Reduction Reactions Involving Electron Transfer. *J. Chem. Phys.* **1956**, *24* (5), 996–978.

(19) Santos, E.; Nazmutdinov, R.; Schmickler, W. Electron Transfer at Different Electrode Materials: Metals, Semiconductors, and Graphene. *Curr. Opin. Electrochem.* **2020**, *19*, 106–112

(20) Huang, J.; Chen, Y. Combining Theory and Experiment in Advancing Fundamental Electrocatalysis. *Curr. Opin. Electrochem.* **2019**, *14*, A4–A9

(21) Hammer, B.; Norskov, J. K. Why Gold Is the Noblest of All the Metals. *Nature* **1995**, *376*, 238–240.

(22) Schalenbach, M.; Kasian, O.; Ledendecker, M.; Cherevko, S.; Mingers, A.; Speck, F.; Mayrhofer, K. J. J. The Electrochemical Dissolution of Noble Metals in Alkaline Media. *Electrocatalysis* **2018**, *9* (2), 153–161.

(23) Cherevko, S.; Topalov, A. A.; Katsounaros, I.; Mayrhofer, K. J. J. Electrochemical Dissolution of Gold in Acidic Medium. *Electrochem. commun.* **2013**, *28*, 44–46

(24) Łukaszewski, M.; Kuśmierczyk, K.; Kotowski, J.; Siwek, H.; Czerwiński, A. Electrosorption of Hydrogen into Palladium-Gold Alloys. *J. Solid State Electrochem.* **2003**, *7* (2), 69–76

(25) Furuya, N.; Koide, S. HYDROGEN ADSORPTION ON PLATINUM SINGLE-CRYSTAL SURFACES. *Surf. Sci.* **1989**, *220*, 18–20

(26) Hamelin, A. Cyclic Voltammetry at Gold Single-Crystal Surfaces. Part 1. Behaviour at Low-Index Faces. *J. Electroanal. Chem.* **1996**, *407* (1–2), 1–11

(27) Piela, B.; Wrona, P. Capacitance of the Gold Electrode in 0.5 M H_2SO_4 Solution: A.c. Impedance Studies. *J. Electroanal. Chem.* **1995**, *388*, 69–79.

(28) Motheo, A. J.; Sadkowski, A.; Neves, R. S. Electrochemical Immittance Spectroscopy Applied to the Study of the Single Crystal Gold/ Aqueous Perchloric Acid Interface. *J. Electroanal. Chem.* **1997**, *430*, 253–262.

(29) Motheo, A. J.; Santos, J. R.; Sadkowski, A.; Hamelin, A. The Gold (210) / Perchloric Acid Interface: Impedance Spectroscopy. *J. Electroanal. Chem.* **1995**, *397*, 331–334.

(30) Pajkossy, T. Capacitance Dispersion on Solid Electrodes: Anion Adsorption Studies on Gold Single Crystal Electrodes. *Solid State Ionics* **1997**, *94* (1–4), 123–129

(31) Pajkossy, T. Impedance Spectroscopy at Interfaces of Metals and Aqueous Solutions - Surface Roughness, CPE and Related Issues. *Solid State Ionics* **2005**, *176* (25–28), 1997–2003

(32) Schmid, G. M.; Hackerman, N. Double Layer Capacities of Single Crystals of Gold in Perchloric Acid Solutions. *J. Electrochem. Soc.* **1962**, *109* (3), 243–247. https://doi.org/10.1149/1.2425380.

(33) Berkes, B. B.; Maljusch, A.; Schuhmann, W.; Bondarenko, A. S. Simultaneous Acquisition of Impedance and Gravimetric Data in a Cyclic Potential Scan for the Characterization of Nonstationary Electrode/Electrolyte Interfaces. *J. Phys. Chem. C* **2011**, *115* (18), 9122–9130

(34) Hamelin, A. The Surface State and the Potential of Zero Charge of Gold (100): A Further Assessment. *J. Electroanal. Chem.* **1995**, *386* (1–2), 1–10

(35) Eberhardt, D.; Santos, E.; Schmickler, W. Impedance Studies of Reconstructed and Non-Reconstructed Gold Single Crystal Surfaces. *J. Electroanal. Chem.* **1996**, *419* (1), 23–31

(36) Fawcett, W. R.; Kováčová, Z.; Motheo, A. J.; Foss, C. A. Application of the Ac Admittance Technique to Double-Layer Studies on Polycrystalline Gold Electrodes. *J. Electroanal. Chem.* **1992**, *326* (1–2), 91–103

(37) Zoltowski, P. On the Electrical Capacitance of Interfaces Exhibiting Constant Phase Element Behaviour. *Electroanal. Chem.* **1998**, *443*, 149–154

(38) Tymosiak-Zielińska, A.; Borkowska, Z. Double Layer Capacitance of Pt(111) Single Crystal Electrodes. *Electrochim. Acta* **2001**, *46* (20–21), 3063–3071

(39) Leikis, D.; Rybalka, K.; Sevatyanov, E.; Frumkin, A. Determination of the Potetnials of Zero Charge of Solid Metals by Means of Differential Capacity Measurements. *Electroanal. Chem. Interfacial Electrochem.* **1973**, *46*, 161–169.

(40) Pell, W. G.; Zolfaghari, A.; Conway, B. E. Capacitance of the Double-Layer at Polycrystalline Pt Electrodes Bearing a Surface-Oxide Film. *J. Electroanal. Chem.* **2002**, *532* (1–2), 13–23

(41) Jorcin, J.-B.; Orazem, M. E.; Pébère, N.; Tribollet, B. CPE Analysis by Local Electrochemical Impedance Spectroscopy. *Electrochim. Acta* **2006**, *51* (8–9), 1473–1479

(42) Hirschorn, B.; Orazem, M. E.; Tribollet, B.; Vivier, V.; Frateur, I.; Musiani, M. Constant-Phase-Element Behavior Caused by Resistivity Distributions in Films: I. Theory. *J. Electrochem. Soc.* **2010**, *157* (12), C452–C457

(43) MacDonald, D. D. Reflections on the History of Electrochemical Impedance Spectroscopy. *Electrochim. Acta* **2006**, *51* (8–9), 1376–1388

(44) Brug, G. J.; van den Eeden, A. L. G.; Sluyters-Rehbach, M.; Sluyters, J. H. The Analysis of Electrode Impedances Complicated by the Presence of a Constant Phase Element. *J. Electroanal. Chem.* **1984**, *176* (1–2), 275–295

(45) Wang, J. C. Realizations of Generalized Warburg Impedance with RC Ladder Networks and Transmission Lines. *J. Electrochem. Soc.* **1987**, *134* (8), 1915–1920

(46) Chang, B.-Y.; Park, S.-M. Electrochemical Impedance Spectroscopy. *Annu. Rev. Anal. Chem. (Palo Alto. Calif).* **2010**, *3* (6), 207–229

(47) Jonscher, A. K. Dielectric Relaxation in Solids. *J. Phys. D. Appl. Phys.* **1999**, *32* (14), R57–R70

(48) Kaatze, U. The Dielectric Properties of Water in Its Different States of Interaction. *J. Solution Chem.* **1997**, *26* (11), 1049–1112

(49) Hamann, C. H.; Hamnett, A.; Vielstich, W.

Electrochemistry, 2nd ed.; Wiley-VCH, 2007.

(50) Chen, T.; Hefter, G.; Buchner, R. Dielectric Spectroscopy of Aqueous Solutions of KCl and CsCl. *J. Phys. Chem. A* **2003**, *107* (20), 4025–4031

(51) Buchner, R.; Hefter, G. T.; May, P. M. Dielectric Relaxation of Aqueous NaCl Solutions. *J. Phys. Chem. A* **1999**, *103* (1), 8–9

(52) Bockris, J.; Gileadi, E.; Mueller, K. Dielectric Relaxation in the Electric Double Layer. *J. Chem. Phys.* **1966**, *44* (4), 1445–1456

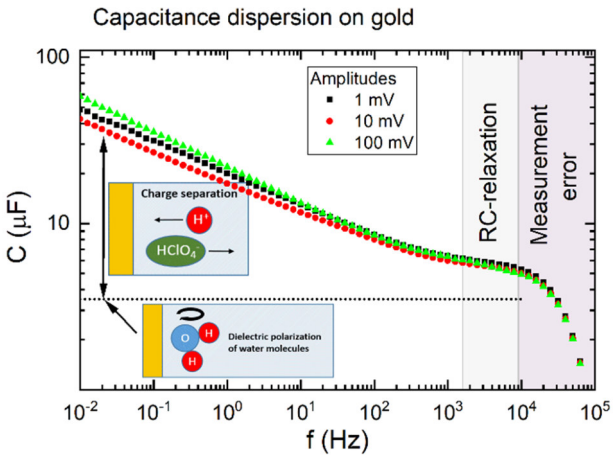

TOC graphic illustration